



Performance of nitrogen-containing macroporous carbon supported cobalt catalyst synthesized through *in-situ* construction of catalytic sites for oxygen reduction reaction

Fan He ^{a, b}, Jun Yang ^a, Rui Li ^c, Bin Hong Liu ^d, Zhou Peng Li ^{a, *}

^a College of Chemical & Biological Engineering, Zhejiang University, Hangzhou, China

^b Department of Chemical Engineering, Massachusetts Institute of Technology, Boston, USA

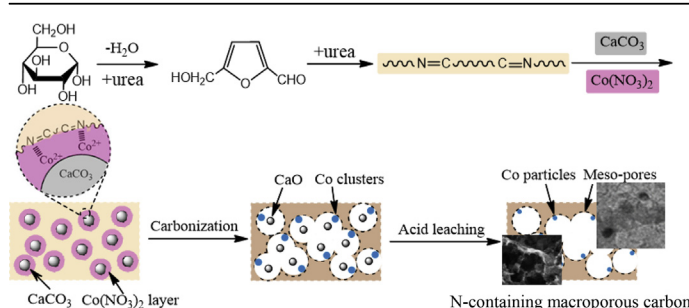
^c Hangzhou No.2 High School of Zhejiang Province, Hangzhou, China

^d Department of Materials Science & Engineering, Zhejiang University, Hangzhou, China

HIGHLIGHTS

- Pyrolysis of composite [glucose-urea resin, nano-CaCO₃, and Co(NO₃)₂] produces superb ORR catalyst comparable to Pt/C.
- CoN_x sites are created simultaneously during formation of N-containing macroporous carbon (N-MPC).
- Decomposition of Co(NO₃)₂ produces mesopores on the macroporous carbon walls.
- The nature of glucose-urea resin significantly influences the catalytic activity of the synthesized Co/N-MPC.

GRAPHICAL ABSTRACT



ARTICLE INFO

Article history:

Received 3 August 2014

Received in revised form

5 October 2014

Accepted 6 October 2014

Available online 15 October 2014

Keywords:

Fuel cell

Cathode catalyst

Catalytic activity

Oxygen reduction reaction

Macroporous carbon

Glucose-urea resin

ABSTRACT

A novel method of *in-situ* catalytic site (CoN_x) construction in macroporous carbon (MPC) is developed. The nitrogen-containing MPC-supported cobalt (Co/N-MPC) catalysts are synthesized *via* the pyrolysis of a mixture of glucose-urea resin, nano-CaCO₃, and cobalt nitrate. The nano-CaCO₃ functions as a template to fabricate MPC that provides high electric conductivity and large specific surface area. The catalytic CoN_x sites are simultaneously created during the formation of N-MPC. The use of glucose-urea resin as the carbon and nitrogen sources significantly increases the nitrogen content as high as 8.8 at% in the MPC. The synthesized Co/N-MPC demonstrates superb catalytic activity toward oxygen reduction reaction. The direct borohydride fuel cell using the Co/N-MPC shows a power density as high as 170 mW cm⁻² which is much higher than the cell using 10 wt.% Pt/C but slightly lower than the cell using 20 wt.% Pt/C as the cathode catalyst at ambient conditions.

© 2014 Elsevier B.V. All rights reserved.

1. Introduction

Fuel cell is regarded as one of the most promising renewable energy conversion devices because of its high efficiency and low pollution [1]. However, the sluggish kinetics of oxygen reduction reaction (ORR) at the cathode and the need for expensive platinum

* Corresponding author. Tel./fax: +86 571 87953149.

E-mail address: zhoupengli@zju.edu.cn (Z.P. Li).

have impeded the commercialization of fuel cells [2]. Thus, developing non-precious metal based catalysts with high efficiency and stability is very important both academically and practically.

Several kinds of non-precious metal ORR catalysts have been developed [3] including metal oxides [4,5], polyoxometalates [6–8], metal sulfides [9], and metal–N₄ macrocyclic compounds such as cobalt phthalocyanine and iron porphyrin compounds [10,11]. Nitrogen-doped carbon-supported catalysts (M–N/C, M stands for metal, N/C for nitrogen-doped carbon support) have attracted much attention because of their high ORR catalytic activities [12–25]. M–N/C catalysts have been successfully synthesized from small molecules [13], macromolecules [14] and polymers [15,16] as a catalyst precursor. Numerous results have shown that the nature of the applied catalyst precursors and the process of the heat treatment are the critical factors that determine the catalytic activity though their mechanisms are not yet fully understood [2,17,18].

The ORR catalytic activity of M–N/C catalysts depends on the surface nitrogen content because nitrogen is the origin of the catalytic sites such as quaternary N, pyridinic N, and CoN_x [19]. The pyrolysis of N-containing organic compounds (such as phthalocyanine, porphyrin and Schiff base [20]) or a catalyst precursor in a nitrogen-rich atmosphere (such as NH₃ and CH₃CN [21]) is a conventional method to create catalytic MN₄ or MN₂ sites [22,23]. N-containing catalytic sites can also be generated by modifying an electroconductive N-containing layer such as polypyrrole (PPy) on a carbon support [24,25]. These studies have proved that the increase in the surface nitrogen content without decreasing the conductivity of the carbon support is a critical issue to improve the catalytic activity.

Carbon support significantly affects catalytic activity toward ORR [19,26] because it functions not only as an active site support but also as an electron conductor. Carbon support also influences the mass transport in the cathode. A carbon support with a large specific surface area (for formation of more catalytic sites) and high electric conductivity (low ohmic resistance) without loss of mass transport capability (small concentration polarization) is preferred. However, a large specific surface area and a high electric conductivity are usually hard to obtain simultaneously in traditional carbon-supported catalysts. For example, the specific surface area of commercialized Pt/C catalysts that utilize XC-72 carbon black as the support is limited to 200 m² g^{−1} because a large specific surface area usually leads to poor electric conductivity, such that the distribution and concentration of the active sites are greatly restricted. The macroporous carbon (MPC) is a potential catalyst support that can solve the contradiction between specific surface area and electric conductivity [27]. MPC prepared with CaCO₃ as the template has been reported to have a specific surface area as high as 1215 m² g^{−1} but its electric resistance is rather low [28].

Traditional M–N/MPC catalysts are usually fabricated by doping a metal source to the nitrogen precursor-modified MPC or doping metal and nitrogen sources to MPC directly [14,29]. However, the full utilization of the abundant inner pores of the MPC is difficult to be achieved by traditional methods. Herein, we explore a novel approach for *in-situ* construction of catalytic sites in the MPC support. The construction of the MPC support, creation of the catalytic sites, and activation of the catalyst are completed in one heat treatment process, which takes advantage of the hierarchical porous structure of the MPC and is more energy-efficient and time-saving than the conventional synthesis method. The Schiff base polymer (glucose-urea resin) coordinating to cobalt is used as the catalyst precursor to increase the nitrogen content in the synthesized catalysts with a large specific surface area. The effects of the synthesized glucose-urea resins on the ORR catalytic activity of the

obtained catalysts are investigated in detail. Finally, the performance of the synthesized catalyst is verified in an alkaline fuel cell for comparison with that of commercialized Pt/C catalysts.

2. Method and procedures

2.1. Catalyst synthesis

Hydroxymethylfurfural (HMF) contains both aldehyde and alcohol functional groups. In the presence of urea, the hydrolysis of glucose generates 5-HMF that polymerizes with urea to form a glucose-urea resin [30]. Glucose monohydrate (11.00 g) and urea (1.67 g) were dissolved in 6 and 2 mL of deionized water, respectively. The urea solution was then added to the glucose solution dropwise and stirred for 40 min at 90 °C to prepare the glucose-urea resin (pre-polymer) until the transparent mixture turned reddish brown. To terminate the polymerization, deionized water (10 mL) was added to the obtained glucose-urea resin. The obtained glucose-urea resin solution was mixed with an emulsion containing 4.64 g of Co(NO₃)₂·6H₂O and 10.00 g of nano-CaCO₃ in 20 mL of deionized water to form a homogeneous suspension. The catalyst precursor was then obtained after 1 h of evaporation at 80 °C.

Further polymerization and subsequent carbonization of the catalyst precursor were performed in a nitrogen atmosphere through the following heating regime: heating from room temperature to 160 °C at a heating rate of 10 °C min^{−1} and holding for 2 h then further heating to 600 °C at the same heating rate and holding for another 2 h. The catalyst precursor was finally heated to 900 °C and held for 2 h and then cooled down to room temperature. Free water and crystal water in Co(NO₃)₂·6H₂O were removed, and polymerization of the glucose-urea resin occurred when heating for 2 h at 160 °C. A relatively fixed composite consisting of the calcined glucose-urea resin and nano-CaCO₃ was produced after 2 h of heating at 600 °C. Decomposition of CaCO₃ and activation of the hierarchical MPC were completed after 2 h of heating at 900 °C. The formed CaO from CaCO₃ decomposition and the redundant cobalt compounds were then removed using an HCl solution (30 wt.%). After ultrasonic treatment and soaking the ground samples in the HCl solution overnight three times, the N-containing MPC-supported cobalt catalyst (Co/N–MPC) was then obtained through overnight drying at 60 °C. The cobalt content was determined by inductively coupled plasma – atomic emission spectroscopy (Varian ICP 725-ES).

2.2. Material characterizations

Fourier transform infrared spectroscopy (FTIR) analysis was conducted to investigate the pre-polymerization of glucose and urea by dissolving the sample in tetrahydrofuran. A Nicolet–IR100 FTIR spectrometer (Cole–Parmer) was used. Thermogravimetric analysis (TGA) was carried out in N₂ at a gas flow rate of 50 mL min^{−1} and a heating rate of 10 °C min^{−1} by using Pyris 1 TGA (Perkin Elmer). The Co/N–MPC structure before and after HCl leaching was identified via X-ray diffraction (XRD, X'Pert PRO PANalytical B.V.) with Cu K α radiation ($\lambda = 1.5406$ Å) from 10° to 80° at a scan rate of 4° min^{−1} with a 0.2 s residence time.

The morphology of the synthesized catalysts was observed via field emission scanning electron microscopy (FESEM, Zeiss Ultra55) at 5 kV and transmission electron microscope (TEM, Hitachi H-9500) at 300 kV. The N₂ adsorption–desorption isotherms of the synthesized samples at 77 K were determined using an Autosorb-1-C automatic surface area analyzer (Quatachrome Corp.). The samples were degassed to 10^{−6} Pa for 2 h at 200 °C before they were tested. Specific surface area, pore size, and pore volume were

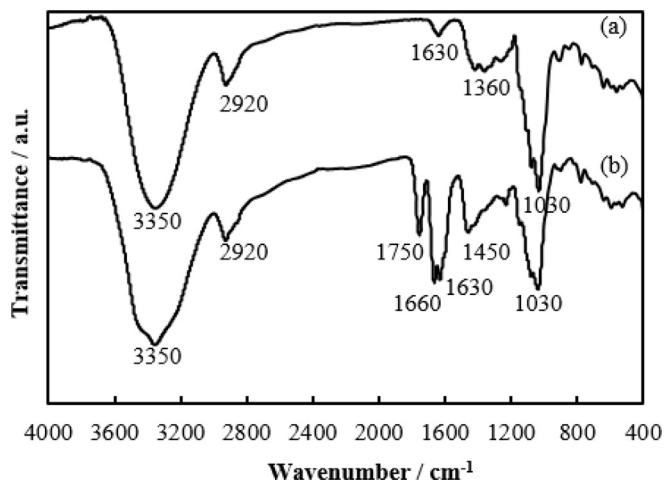


Fig. 1. FTIR spectra of glucose hydrolysis product (a) and glucose-urea resin (b).

calculated based on the Brunauer–Emmett–Teller (BET) and Barret–Joyner–Halenda (BJH) methods. The N species and their relative contents in the Co/N–MPC were determined via X-ray photoemission spectroscopy (XPS) by using a PHI–5000C ESCA system (Perkin Elmer) with Mg K α radiation ($h\nu = 1253.6$ eV). All spectra were referenced to the Cls level at 284.6 eV to correct the peak shift that occurred because of charge accumulation on the sample. Raw data were fitted and deconvoluted using the XPS Peak 4.1 software.

2.3. Electrochemical evaluation

Platinum dissolution occurred when a Pt counter electrode was used in an acidic electrolyte, which influenced the reaction on the working electrode [31]. As such, the catalytic activity of the synthesized catalyst was evaluated in an alkaline electrolyte in the present study. The metal corrosion could be significantly depressed in an alkaline electrolyte. Cyclic voltammograms (CVs) were recorded in a three-electrode system in the 0.1 M KOH solution saturated with O₂ at 25 °C and a scan rate of 10 mV s^{−1} by using a CHI 1140A electrochemical workstation (CH Instruments). The catalyst slurry was prepared by mixing 8.0 mg of the catalyst with 3 mL of ethanol and 0.2 mL of Nafion suspension (5 wt.%) after ultrasonic treatment for 10 min. The working electrode was prepared by coating 20 μ L of the slurry onto a pretreated glassy carbon electrode (3 mm in diameter) and subsequent drying at room temperature. Platinum wire electrode and saturated calomel electrode (SCE) were used as the counter and reference electrode,

respectively. The potentials were converted to the values vs. standard hydrogen electrode (SHE) (SCE = 0.245 V vs. SHE at 25 °C). Linear sweep voltammetry (LSV) analysis was conducted using rotating disk electrode (RDE) (RDE-2, BASi Inc.) to estimate the kinetic current density and electron transfer number of the ORR.

According to Koutecky–Levich's theory [32], the K–L equation is expressed as follows:

$$\frac{1}{I} = \frac{1}{I_k} + \frac{1}{0.62nFA_eC_0D_0^{2/3}\nu^{-1/6}\omega^{1/2}} \quad (1)$$

where I is the disk current, I_k is the kinetic current, ω is the angular frequency of rotation, F is the Faraday constant, A_e is the electroactive area of the applied catalyst, and n is the number of electrons transferred per O₂ molecule via ORR. However, determining the electroactive area is difficult for a porous electrode studied in this work. The n value was then estimated based on the geometric area (A_g) of the disk electrode. Published data of O₂ saturated concentration (C_0), diffusion coefficients (D_0) of O₂ in 0.1 M KOH solution, and kinematic viscosity (ν) of 0.1 M KOH solution were used [33].

Exactly 5 μ L of the catalyst slurry was pipetted onto the polished glass carbon electrode (3 mm in diameter). The RDE LSV curves were recorded between −0.8 and 0.2 V vs. SCE in the 0.1 M KOH solution saturated with O₂ at 25 °C, a scan rate of 10 mV s^{−1}, and rotation rates of 300, 400, 500, 800, and 1300 rpm.

A single fuel cell with an active area of 6 cm² was assembled to evaluate the performance of the synthesized Co/N–MPC. A polyvinylidene fluoride (PVDF) solution in N-methyl-2-pyrrolidone (NMP) was used to coat PVDF into the inner pores of the applied catalyst to improve its hydrophobic property. The catalyst slurry was prepared by mixing the catalyst powder, PVDF solution in NMP (2.5 wt.%), deionized water, and ethanol with a mass ratio of 1:7:3:3. The cathode was prepared by coating 5.0 mg cm^{−2} of the catalyst onto a piece of hydrophobic carbon cloth and then heated at 140 °C for 2 h to improve its hydrophobic property. The anode was prepared by coating the anode catalyst (5.0 mg cm^{−2}) onto a piece of Ni foam. The anode catalyst ink was prepared by mixing the commercial Pt/C (20 wt.%), Nafion solution (5 wt.%), deionized water, and ethanol with a mass ratio of 1:7:3:3. Nafion 211 membrane was used as the electrolyte after sequentially boiled in 3 wt.% H₂O₂ solution, deionized water, 0.5 M H₂SO₄, and deionized water for 30 min. An alkaline NaBH₄ solution (5 wt.% NaBH₄ and 10 wt.% NaOH) was used as the fuel. The cell performance was measured at a fuel flow rate of 10 mL min^{−1} and a dry O₂ flow rate of 150 mL min^{−1} at ambient conditions. The cell configuration and test system were the same as described in a previous work [16].

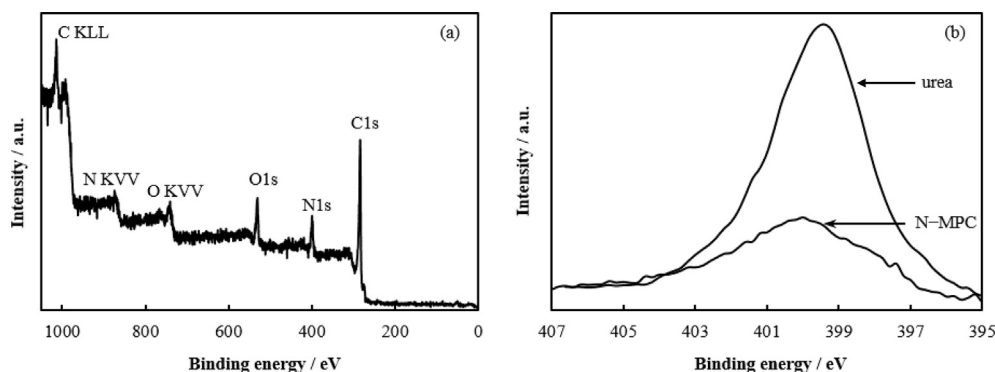


Fig. 2. (a) Full range XPS spectrum of N–MPC and (b) comparison of N1s binding energy in N–MPC and urea.

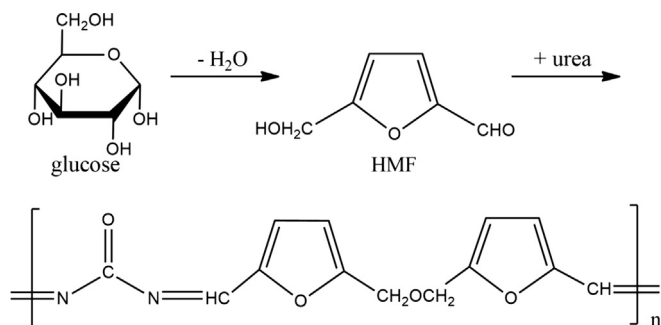


Fig. 3. Polymerization scheme of glucose and urea.

3. Results and discussion

3.1. Glucose-urea resin and macroporous carbon

Fig. 1 shows the FTIR spectra of the synthesized glucose-urea compound. The glucose-urea compound was obtained after heating the glucose-urea solution (50 wt.% of glucose, 17 wt.% of urea) at 90 °C for 40 min with stirring. For comparison, the glucose hydrolysis product was made from the glucose solution (50 wt.%). The peaks at 3350, 2920, 1630, and 1030 cm^{-1} were assigned to the stretching vibrations of N–H and O–H, CH_2 , C=O, and C–O–C, respectively. The synthesized glucose-urea compound presented a new peak appearing at 1750 cm^{-1} , which was assigned to the ester bond in $\text{NH}_2\text{CONHCOO}-\text{R}$. The peak at 1660 cm^{-1} was identified as the vibration of C=N (1590–1690 cm^{-1}), which was the characteristic absorption peak of a Schiff base [34,35]. The FTIR results suggested that the synthesized glucose-urea compound was a polymerized product of glucose and urea (glucose-urea resin).

The N–MPC was prepared after the removal of CaO in the calcined mixture of the glucose-urea resin and nano- CaCO_3 with a mass ratio of 1:1. The glucose-urea resin was obtained through polymerization as described above. The nitrogen existence was

Table 1

Specific surface area and pore characterization of synthesized carbon materials.

	XC-72	MPC	N-MPC	Co/N-MPC
Mean pore diameter/nm	8	19	9	20
Pore volume/ $\text{cm}^3 \text{g}^{-1}$	0.43	3.39	1.46	3.01
Specific surface area/ $\text{m}^2 \text{g}^{-1}$	216	699	714	608

conformed as shown in the full range XPS spectrum (Fig. 2). The N1s binding energy in N–MPC (400.0 eV) was higher than that in urea (399.2 eV). This result indicated that the amino nitrogen bond ($-\text{NH}_2$) in urea was broken. A strong bond (N–C) was formed in the N–MPC. Both FTIR and XPS results revealed that glucose was first hydrolyzed into 5-HMF in the urea solution, and then the produced 5-HMF reacted with urea to form a Schiff base polymer during heating at 90 °C, as shown in the reaction scheme in Fig. 3. The measured nitrogen content in the N–MPC was as high as 8.8 at%. The use of the glucose-urea resin as the nitrogen precursor for M/N–MPC synthesis was an effective way to obtain the catalysts with high nitrogen content.

Fig. 4 shows the morphologies of the MPC made from glucose [Fig. 4(a)] and the N–MPC made from glucose-urea resin [Fig. 4(b)]. The mean pore diameters of the mesopores and macropores in the MPC were calculated to be 19 and 200 nm, respectively. The measured pore volume and the specific surface area of the MPC were 3.39 $\text{cm}^3 \text{g}^{-1}$ and 699 $\text{m}^2 \text{g}^{-1}$, respectively. These values were much larger than the values obtained from the commercialized carbon support XC-72 (Table 1). The large values of pore volume and specific surface area implied that the obtained MPC had a smaller mass transfer resistance. However, N–MPC had a smaller mean pore diameter and pore volume but a slightly larger specific surface area than the MPC. The smaller mean pore diameter and pore volume may possibly lead to the increase in mass transfer resistance in the N–MPC based catalysts. To compensate such decreases in pore size and volume, $\text{Co}(\text{NO}_3)_2 \cdot 6\text{H}_2\text{O}$ (transition metal precursor) was then used as an auxiliary pore-forming agent. Mesopores were successfully produced on the carbon walls in Co/

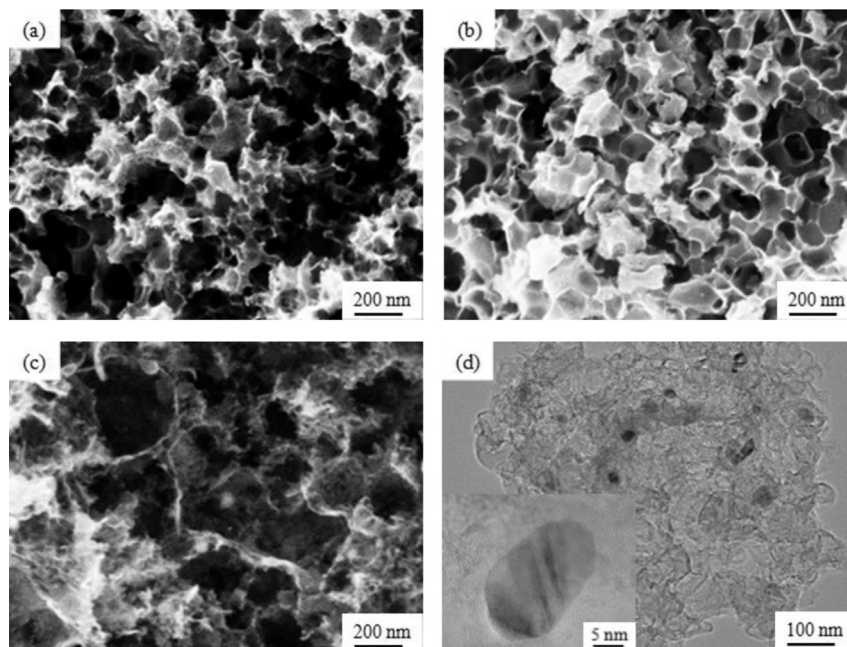


Fig. 4. SEM images of (a) MPC made from glucose, (b) N–MPC made from glucose-urea resin, (c) Co/N–MPC, and (d) TEM image of Co/N–MPC, using nano- CaCO_3 as the template. Inset is the HRTEM of Co/N–MPC.

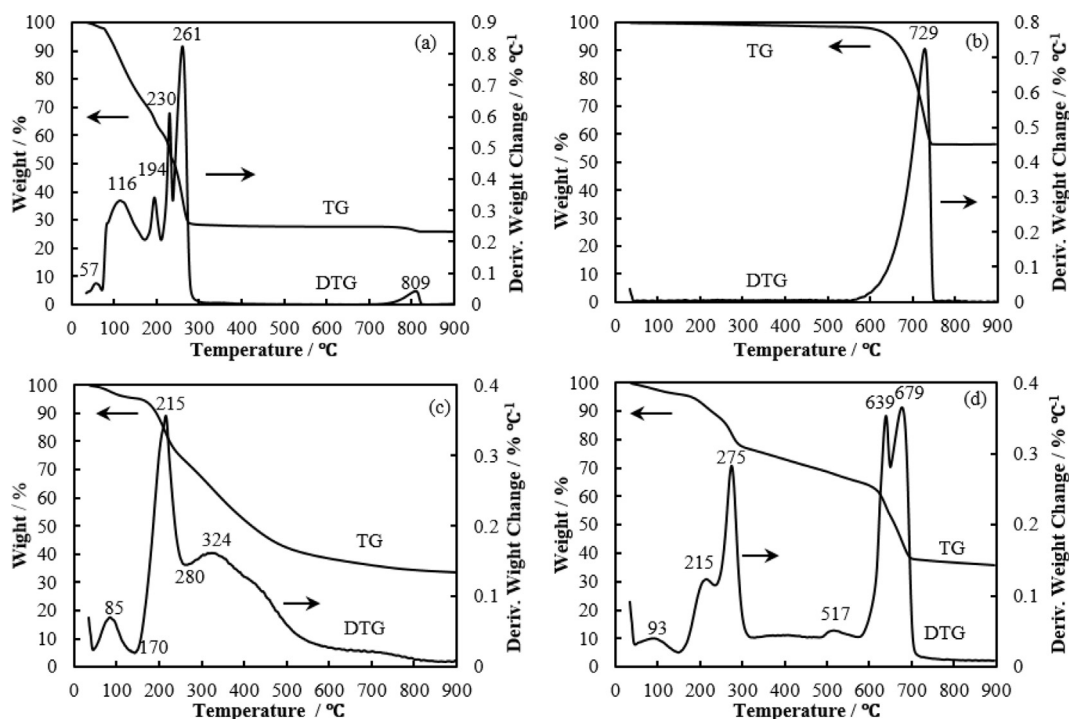
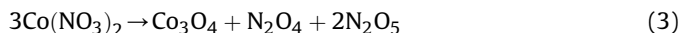
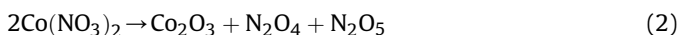


Fig. 5. TG and DTG curves of (a) $\text{Co}(\text{NO}_3)_2 \cdot 6\text{H}_2\text{O}$, (b) nano- CaCO_3 , (c) glucose-urea resin, and (d) catalyst precursor [mixture of $\text{Co}(\text{NO}_3)_2 \cdot 6\text{H}_2\text{O}$, nano- CaCO_3 and glucose-urea resin] at a heating rate of $10^\circ\text{C min}^{-1}$. Mole ratio of glucose to urea for the resin synthesis is 2:1.

N-MPC, as shown in Fig. 4(c). The pore structure data confirmed that Co/N-MPC had a comparable pore size and volume to MPC (Table 1).

3.2. Nitrogen contained MPC supported cobalt catalyst

The TG curves of each raw material for Co/N-MPC synthesis are shown in Fig. 5. From the differential thermogravimetric (DTG) curve of the cobalt nitrate hexahydrate [Fig. 5(a)], peaks at 57, 116, and 194°C were assigned to the dehydration of $\text{Co}(\text{NO}_3)_2 \cdot 6\text{H}_2\text{O}$, $\text{Co}(\text{NO}_3)_2 \cdot 4\text{H}_2\text{O}$, $\text{Co}(\text{NO}_3)_2 \cdot 2\text{H}_2\text{O}$, respectively [36]. The DTG peaks at 230, 261, and 809°C were attributed to the sequent decomposition of $\text{Co}(\text{NO}_3)_2$ [37], as described as follows:



The removal of water (produced in polymerization of glucose and urea) proceeded during heating from room temperature to 170°C [Fig. 5(c)]. Further heating to 280°C led to the deep polymerization of the glucose-urea resin to release more water. The first and second decompositions of $\text{Co}(\text{NO}_3)_2$ [Reaction (2), (3)] happened when the deep polymerization of the glucose-urea resin proceeded at 170 – 280°C . Therefore, the formation of the mesopores on the carbon walls was mainly caused by the decomposition of $\text{Co}(\text{NO}_3)_2$.

The carbonization of the glucose-urea resin started around 300°C . Nano- CaCO_3 decomposition occurred at 600°C forming macropores [Fig. 5(b)]. The weight of the pyrolyzed remnant

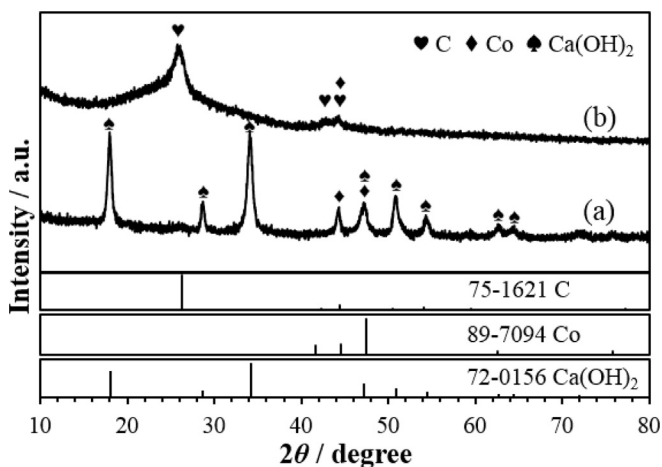


Fig. 6. XRD patterns of the prepared Co/N-MPC before (a) and after (b) HCl leaching.

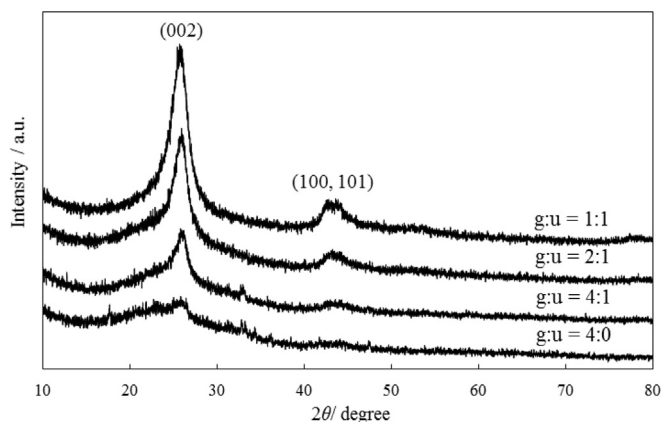


Fig. 7. XRD patterns of Co/N-MPC made from the glucose-urea resins with different mole ratios of glucose to urea.

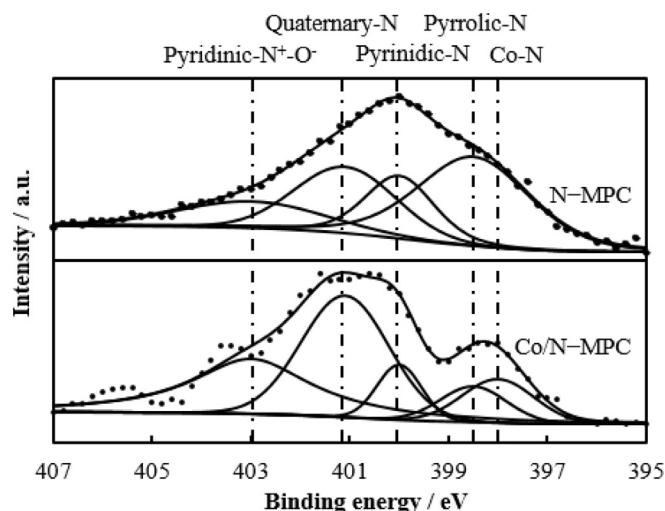


Fig. 8. High resolution N1s spectra of N-MPC and Co/N-MPC made from glucose-urea resin. Mole ratio of glucose to urea for the resin synthesis is 2:1.

decreased to 56% of the original weight, thereby indicating that CaCO_3 was decomposed into CaO and CO_2 . The generated CO_2 functioned as an active gas that made pores connected and enlarged. Heating from 700 to 900 °C led to the reduction of Co_3O_4 forming metallic Co [18]. The Co/N-MPC catalyst was then obtained after leaching CaO and the redundant cobalt compounds away from the pyrolyzed product with an HCl solution.

Metallic Co and $\text{Ca}(\text{OH})_2$ instead of CaO were detected in the pyrolyzed product (as shown in Fig. 6). $\text{Ca}(\text{OH})_2$ originated from CaO that absorbed the moisture in air before XRD analysis. After HCl leaching, nano-Co and graphitized carbon were detected [Figs. 4(d) and 7]. The broad XRD diffraction peaks at 26.1, 43.4, and 44.3° were assigned to (002), (100) and (101) planes of graphite. The Co/MPC made from glucose showed an amorphous feature (low graphitization degree). When the urea content in the resin was increased (glucose: urea = 4:0, 4:1, 2:1, 1:1), the (100) and (101) peak heights increased and the (002) peak became strong and sharp. These results revealed that the graphitization degree of the obtained Co/N-MPC was significantly improved when more urea was added during polymerization [24]. The increase in the graphitization degree of the Co/N-MPC improved the electronic conductivity [28], which was very important to enhance ORR.

Fig. 8 shows the normalized N1s core level spectra of N-MPC and Co/N-MPC. The N1s spectrum of N-MPC displays four peaks assigned to pyridinic- N^+-O^- (403.0 eV), quaternary N (401.1 eV), pyrrolic N (400.0 eV), and pyridinic N (398.5 eV) after spectral deconvolution [38–41]. Compared to the N1s spectrum of N-MPC, that of Co/N-MPC clearly presents a peak at lower binding energy (398.0 eV), which is assigned to the Co–N bond [41]. The relative contents of pyridinic- N^+-O^- , quaternary N, pyrrolic N, pyridinic N and CoN_x in the Co/N-MPC catalyst are listed in Table 2. The relative content of each N-species is determined by the corresponding peak area after spectral deconvolution and normalization. The Co/N-MPC catalyst exhibited higher contents of pyridinic- N^+-O^- ,

Table 2

Relative contents (at.%) of N-species in the N-MPC and Co/N-MPC.

	Pyridinic- N^+-O^-	Quaternary-N	Pyrrolic-N	Pyridinic-N	Co-N
N-MPC	11.9	25.7	25.6	36.7	–
Co/N-MPC	38.9	41.8	9.7	9.7	12.4

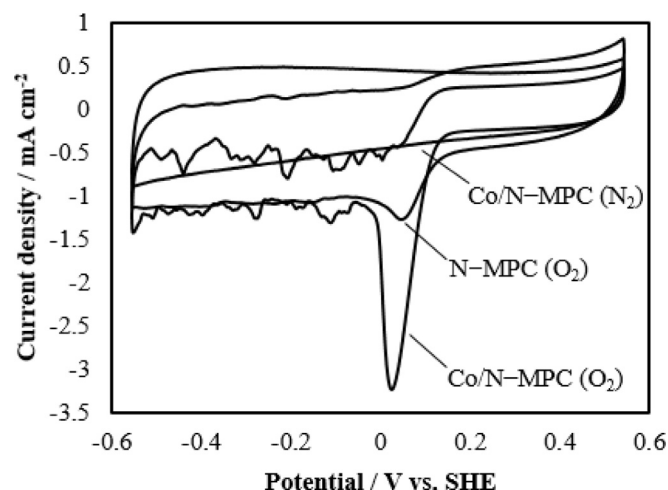


Fig. 9. Cyclic voltammograms of N-MPC and Co/N-MPC in N_2 and O_2 saturated 0.1 M KOH solution. Scan rate: 10 mV s^{-1} , temperature: 25 °C.

quaternary N and CoN_x but lower pyrrolic N and pyridinic N contents than N-MPC. The high contents of quaternary N and CoN_x in Co/N-MPC are the key to enhance ORR because they catalyze ORR more effectively [42,43].

3.3. Electrochemical characterization of the Co/N-MPC catalyst

N-MPC showed poor catalytic activity toward ORR (Fig. 9) though it contained 8.8 at% of nitrogen and had a large portion of pyridinic N (36.7%). Co/N-MPC (containing CoN_x and more quaternary N but less pyridinic N than N-MPC) exhibited a much higher catalytic activity than N-MPC, thereby indicating that CoN_x catalyzed ORR more effectively than pyridinic N. The increase in nitrogen content in the catalyst precursor enhanced the formation of CoN_x [44].

Fig. 10 shows the CVs of the Co/N-MPC made from the glucose-urea resins with different mole ratios of glucose to urea. The Co/MPC made from the pyrolysis of glucose and Co nitrate showed sluggish ORR kinetics (lower ORR current). The ORR current and onset potential increased when the urea content was increased (the mole ratio of glucose to urea changed from 4:0 to 2:1). However, further increase in the urea content showed little effect on the ORR

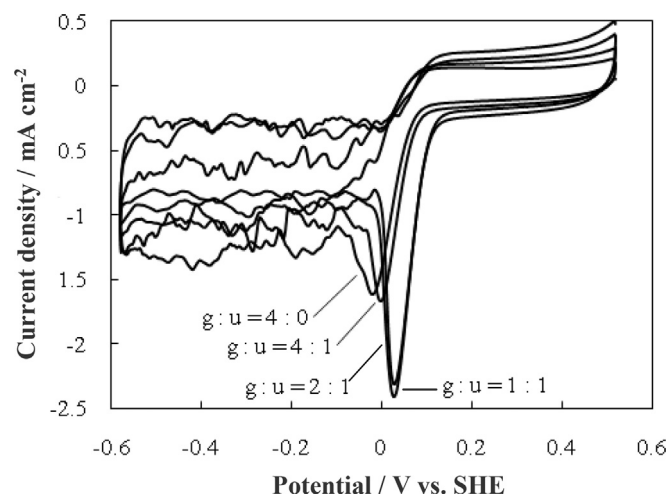


Fig. 10. Cyclic voltammograms of Co/N-MPC made from glucose-urea resins with different mole ratios of glucose to urea. Scan rate: 10 mV s^{-1} , temperature: 25 °C.

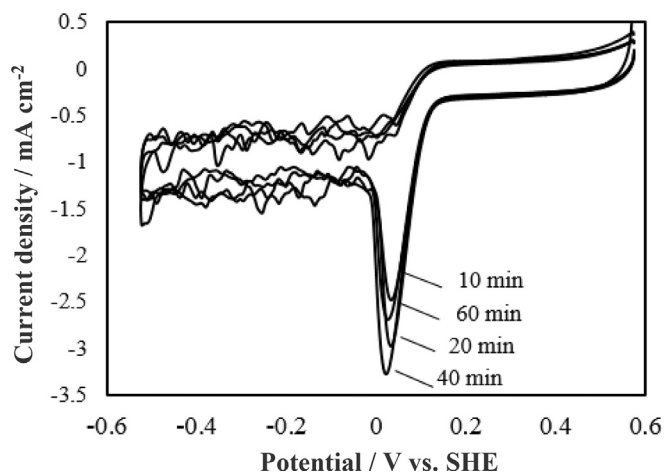


Fig. 11. Cyclic voltammograms of Co/N-MPC made from glucose-urea resins with different pre-polymerization time. Scan rate: 10 mV s^{-1} , temperature: 25°C .

current improvement. The increase in the graphitization degree of the Co/N-MPC caused by the increase in urea content during polymerization also enhanced the ORR because of the electronic conductivity improvement.

Polymerization degree is another factor that affects the nitrogen content in the ORR catalysts when N-containing polymers are used as the nitrogen source [45]. Fig. 11 shows the CVs of the Co/N-MPCs obtained from the glucose-urea resins with different pre-polymerization time. Increasing the pre-polymerization time of the glucose-urea resin up to 40 min led to the increase in the ORR current of Co/N-MPC, whereas its onset potential changed insignificantly. However, further increasing the pre-polymerization time to 60 min caused deep polymerization of the glucose-urea resin, which led to the poor dissolution of the synthesized glucose-urea resin in water. As a result, the ORR activity of Co/N-MPC was significantly deteriorated. Therefore, the use of the glucose-urea resins synthesized through proper pre-polymerization time (with proper molecular weight) as the catalyst precursor was very important to improve the catalytic activity of the Co/N-MPC.

Fig. 12 shows the RDE LSV curves of Co/N-MPC made from the glucose-urea resin after 40 min of pre-polymerization (the mole ratio of glucose to urea in the resin is 2:1) and the corresponding K–L plots at -0.10 V vs. SHE . The limiting current of Co/N-MPC was higher than that of Pt/C containing 10 wt.% of Pt but lower than Pt/C containing 20 wt.% of Pt [Fig. 12(a)]. The calculated kinetic current

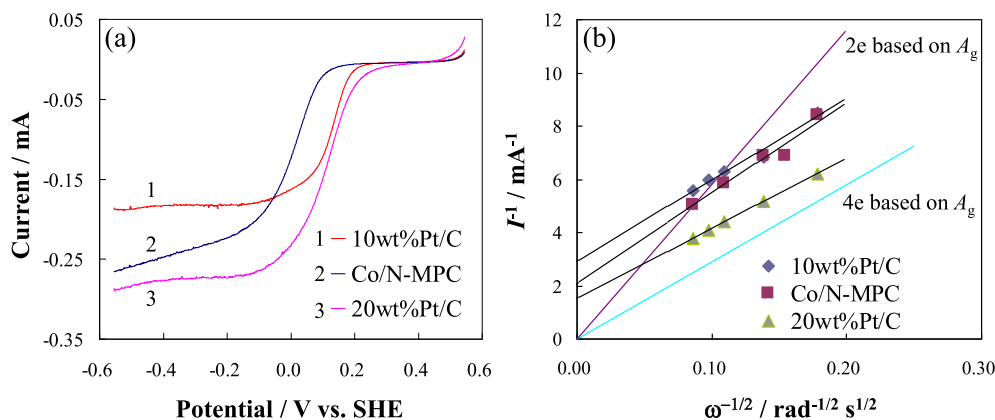


Fig. 12. (a) RDE LSV curves of Co/N-MPC (Co content: 0.33 wt.%), 10 wt.% Pt/C and 20 wt.% Pt/C in O_2 saturated 0.1 M KOH solution at a rotation rate of 1300 rpm. Scan rate: 10 mV s^{-1} , temperature: 25°C . (b) The corresponding K–L plots at -0.10 V vs. SHE .

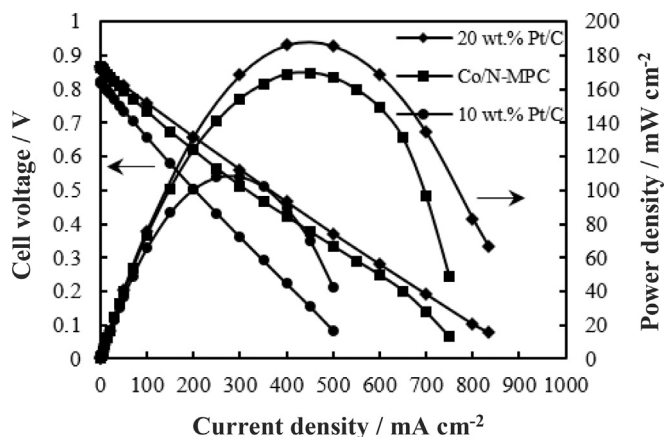


Fig. 13. Performance of the DBFC using Co/N-MPC (Co content: 0.33 wt.%), 10 wt.% Pt/C and 20 wt.% Pt/C as the cathode catalyst at ambient conditions. Catalyst loading in cathode and anode: 5 mg cm^{-2} , Anode catalyst: 20 wt.% Pt/C, electrolyte: Nafion 211. Fuel: 5 wt.% NaBH_4 and 10 wt.% NaOH solution at a flow rate of 10 mL min^{-1} . Dry O_2 at 150 mL min^{-1} .

density ($j_k = I_k/A_{\text{BET}}$) of ORR at Co/N-MPC was 0.006 mA cm^{-2} which was much smaller than the values obtained from the 10 wt.% Pt/C (0.012 mA cm^{-2}) and 20 wt.% Pt/C (0.023 mA cm^{-2}). A_{BET} is the surface area of the applied catalyst on the RDE, as measured via the BET method. Pt/C catalyzed the ORR via the 4e transfer pathway. However, the calculated n value obtained from Co/N-MPC was 3.4, thereby indicating that the ORR on the Co/N-MPC proceeded at different catalytic sites simultaneously, probably via the 2e pathway at the pyridinic N and via the 4e pathway at the CoN_x [44].

Fig. 13 shows the performance of the DBFC with the synthesized Co/N-MPC catalyst. A peak power density of 170 mW cm^{-2} was achieved at ambient conditions, which was higher than the performance of the cell with commercial 10 wt.% Pt/C catalyst (109 mW cm^{-2}) and close to the performance of the cell with 20 wt.% Pt/C catalyst (186 mW cm^{-2}).

4. Conclusions

The N-containing MPC-supported cobalt (Co/N-MPC) catalysts were synthesized via the pyrolysis of composites containing glucose-urea resin, nano- CaCO_3 , and cobalt nitrate. The decomposition of $\text{Co}(\text{NO}_3)_2$ produced mesopores on the macroporous carbon walls. Catalytic CoN_x sites were simultaneously created during the formation of N-containing MPC. The nature of glucose-urea resin

significantly influenced the catalytic activity of the synthesized Co/N-MPC. Pre-polymerization time and mole ratio of glucose to urea dominated the catalytic activity because they changed the molecular weight of the resin and the graphitization degree of Co/N-MPC. The use of glucose-urea resin as the carbon and nitrogen sources is an effective way to increase the nitrogen content in Co/N-MPC.

The synthesized Co/N-MPC from the glucose-urea resin after 40 min of pre-polymerization (mole ratio of glucose to urea = 2:1) demonstrated superb oxygen reduction reaction activity. The direct borohydride fuel cell with Co/N-MPC showed a power density as high as 170 mW cm^{-2} , which was much higher than the cell with 10 wt.% Pt/C but slightly lower than the cell with 20 wt.% Pt/C as the cathode catalyst at ambient conditions.

Acknowledgments

This work is financially supported by the National Natural Science Foundation of China, Grant Nos. 21476200, 21276229 and 51271164; the Zhejiang Provincial Natural Science Foundation of China, Grant No. Z4110126; the Doctoral Fund from the Education Ministry of China (20100101110042).

References

- [1] S. Haile, *Acta Mater.* 51 (2003) 5981–6000.
- [2] F. Jaouen, E. Proietti, M. Lefevre, R. Chenitz, J. Dodelet, G. Wu, H. Chung, C. Johnston, P. Zelenay, *Energy Environ. Sci.* 4 (2011) 114–130.
- [3] Z.P. Li, B.H. Liu, *J. Appl. Electrochem.* 40 (2010) 475–483.
- [4] Y. Gorlin, T. Jaramillo, *J. Am. Soc.* 132 (2010) 13612–13614.
- [5] Y. Gorlin, T. Jaramillo, *ECS Trans.* 41 (2011) 1701–1707.
- [6] B.R. Limoges, Ronald J. Stanis, J.A. Turner, A.M. Herring, *Electrochim. Acta* 50 (2005) 1169–1179.
- [7] M.C. Kuo, R.J. Stanis, J.R. Ferrell III, J.A. Turner, A.M. Herring, *Electrochim. Acta* 52 (2007) 2051–2061.
- [8] C. Gu, C. Shannon, *J. Mol. Catal. A Chem.* 262 (2007) 185–189.
- [9] L. Zhang, J. Zhang, D. Wilkson, H. Wang, *J. Power Sources* 156 (2006) 171–182.
- [10] R. Jasinski, *Nature* 201 (1964) 1212–1213.
- [11] R. Bashyam, P. Zelenay, *Nature* 443 (2006) 63–66.
- [12] C. Bezerra, L. Zhang, K. Lee, H. Liu, A. Marques, E. Marques, H. Wang, J. Zhang, *Electrochim. Acta* 53 (2008) 4937–4951.
- [13] H. Wang, R. Cote, G. Faubert, D. Guay, J.P. Dodelet, *J. Phys. Chem. B* 103 (1999) 2042–2049.
- [14] G. Lalande, R. Cote, G. Ramizhmani, D. Guay, J. Dodelet, L. Dignard-Bailey, L. Weng, P. Bertrand, *Electrochim. Acta* 40 (1995) 2635–2646.
- [15] S. Gupta, D. Tryk, I. Bae, W. Aldred, E. Yeager, *J. Appl. Electrochem.* 19 (1989) 19–27.
- [16] H.Y. Qin, Z.X. Liu, L.Q. Ye, J.K. Zhu, Z.P. Li, *J. Power Sources* 192 (2009) 385–390.
- [17] J.A.R. van Veen, H.A. Colijn, J. van Baar, *Electrochim. Acta* 33 (1988) 801–804.
- [18] H.Y. Qin, S.J. Lao, Z.X. Liu, J.K. Zhu, Z.P. Li, *Int. J. Hydrogen Energy* 35 (2010) 1872–1878.
- [19] Z.P. Li, Z.X. Liu, K.N. Zhu, Z. Li, B.H. Liu, *J. Power Source* 219 (2012) 163–171.
- [20] R. Cote, G. Lalande, G. Faubert, D. Guay, J.P. Dodelet, G. Denes, *J. Electrochem. Soc.* 145 (1998) 2411–2418.
- [21] G. Faubert, R. Cote, J. Dodelet, M. Lefevre, P. Bertrand, *Electrochim. Acta* 44 (1999) 2589–2603.
- [22] A. Bouwkamp-Wijnoltz, W. Visscher, J. van Veen, E. Boellaard, A. van der Kraan, S. Tang, *J. Phys. Chem. B* 106 (2002) 12993–13001.
- [23] M. Lefevre, J. Dodelet, P. Bertrand, *J. Phys. Chem. B* 106 (2002) 8705–8713.
- [24] A. Bouwkamp-Wijnoltz, W. Visscher, J. van Veen, S. Tang, *Electrochim. Acta* 45 (1999) 379–386.
- [25] M. Yuasa, A. Yamaguchi, H. Itsuki, K. Tanaka, M. Yamamoto, K. Oyaizu, *Chem. Mater.* 17 (2005) 4278–4281.
- [26] H.Y. Qin, Z.X. Liu, S.J. Lao, J.K. Zhu, Z.P. Li, *J. Power Sources* 195 (2010) 3124–3129.
- [27] C. Zhao, W. Wang, Z. Yu, H. Zhang, A. Wang, Y. Yang, *J. Mater. Chem.* 20 (2010) 976–980.
- [28] G. Xu, Y. Xu, J. Fang, X. Peng, F. Fu, L. Huang, J. Li, S. Sun, *ACS Appl. Mater. Interfaces* 5 (2013) 10782–10793.
- [29] G. Wei, J.S. Wainright, R.F. Savinell, *J. New. Mater. Electrochem. Syst.* 3 (2000) 121–130.
- [30] T. Viswanathan, T. Richardson, *Ind. Eng. Chem. Res.* 23 (1984) 644–647.
- [31] C. Gu, B.C. Norris, F.F. Fan, C.W. Bielawski, A.J. Bard, *ACS Catal.* 2 (2012) 746–750.
- [32] A.J. Bard, L.R. Faulkner, *Electrochemical Methods: Fundamentals and Application*, second ed., John Wiley & Sons, Inc, New York, 2001, p. 341.
- [33] D. Zhang, D. Chi, T. Okajima, T. Ohsaka, *Electrochim. Acta* 52 (2007) 5400–5406.
- [34] S. Zolezzi, A. Decinti, E. Spodine, *Polyhedron* 18 (1999) 897–904.
- [35] S. Chen, L. Zhang, *Sci. China Ser. B* 48 (2005) 29–32.
- [36] C. Ehrhardt, M. Gjikaj, W. Brockner, *Thermochim. Acta* 432 (2005) 36–40.
- [37] S. Yuvaraj, L. Fan-Yuan, C. Tsong-Huei, Y. Chuin-Tih, *J. Phys. Chem. B* 107 (2003) 1044–1047.
- [38] G. Liu, X. Li, P. Ganesan, B. Popov, *Appl. Catal. B Environ.* 93 (2009) 156–165.
- [39] K. Lee, L. Zhang, H. Lui, R. Huim, Z. Shi, J. Zhang, *Electrochim. Acta* 54 (2009) 4704–4711.
- [40] H. Wang, T. Maiyalagan, X. Wang, *ACS Catal.* 2 (2012) 781–794.
- [41] Z.X. Liu, B.H. Liu, Z.P. Li, *Int. J. Hydrogen Energy* 39 (2014) 5689–5695.
- [42] H.-S. Oh, J.-G. Oh, B. Roh, I. Huang, H. Kim, *Electrochem. Commun.* 13 (2011) 879–881.
- [43] S. Kundu, T. Nagaiah, W. Xia, Y. Wang, S. Dommele, J. Bitter, M. Santa, G. Grundmeier, M. Bron, W. Schuhmann, M. Muhleret, *J. Phys. Chem. C* 113 (2009) 14302–14310.
- [44] H.Y. Qin, K.N. Zhu, L.Q. Ye, Zhou Peng Li, *J. Power Sources* 208 (2012) 203–209.
- [45] Y. Wang, X.C. Wang, M. Antonietti, *Angew. Chem. Int. Ed.* 51 (2012) 68–89.